Monthly Performance of a Photovoltaic Thermal System in Series with a Solar Thermal Collector in Laminar and Turbulent Regimes

Jabri, Ali; Ansari Mohammad, Reza*+; Maerefat, Mehdi
Department of Mechanical Engineering, Tarbiat Modares University, Tehran, I.R. IRAN

ABSTRACT: *Solar thermal (ST) collectors could only generate thermal power, while photovoltaic thermal (PVT) systems could provide both electricity and thermal power. However, the PVTs outlet temperature is usually not high enough for use in many applications such as space heating. Therefore, a new system called PVT system and ST collector in series (PVT-ST) is inducted to generate thermal power with higher outlet temperature and electricity. This paper explores the potential and feasibility of using PVT-ST under relatively hot and dry weather conditions in four cities of Tehran, Abadan, Baghdad, and Basra. To this end, the yearly performance of the system in terms of the first and second laws of thermodynamics is numerically evaluated. Moreover, the effects of the working fluid mass flow rate, in both laminar and turbulent regimes, on the module performance are investigated. Additionally, a comparative study is made between the PVT-ST, single PVT, and single ST systems. The working fluid regime analysis reveals that optimal thermal and electrical efficiency can be obtained in a turbulent regime. While the turbulent regime reflects better electrical exergy, the thermal exergy is dramatically decreased by raising the mass flow rate. Considering the mass flow rate of 0.0304 kg/s (turbulent regime) in July, the thermal efficiencies of the single ST, PVT-ST, and single PVT systems are 85.7%, 78%, and 72.9%, respectively. However, regardless of the mass flow rate, the PVT-ST system has the highest thermal exergy, peaking at 14.56 W/m^2 at the lowest mass flow rate (laminar regime), which is double the thermal exergy of the single PVT. Finally, the annual study of the system performance in different cities illustrates that the maximum thermal power and exergy can be produced in Basra, averaging 375.72 and 1.46 W/m^2. However, the maximum electricity production, with an average of 77 W/m^2 belongs to Baghdad.*

KEYWORDS: *Photovoltaic thermal system; Thermal and electrical power; Energy and exergy analyses; Solar thermal collector*.

INTRODUCTION

To cope with environmental concerns due to using fossil fuels and the daily demand increase for energy, replacing renewable energy resources, e.g., solar, hydropower, bioenergy, and wind with fossil fuels has

**To whom correspondence should be addressed.*
+ E-mail: mra_1330@modares.ac.ir
1021-9986/2023/10/1733-3536 17/$/6.07

been widely considered. Among diverse sources of renewable energies, solar energy has attracted more attention thanks to being unlimited and accessible worldwide [1]. The total solar radiation received by our planet is approximately 15000 times the overall energy consumed around the world [2]. Therefore, to benefit from this valuable source of energy, many technologies are developed to convert solar radiation to different types of energy. As one of the most popular solar systems, photovoltaic (PV) technology is developed to convert solar radiation into electricity. Many researchers have studied the performance of these systems and suggested different ways to improve their performance [3].

Furthermore, in order to use solar radiation in the form of thermal energy, solar thermal (ST) collectors are designed [4]. In these systems, the solar radiation is absorbed by an absorber plate/tube and then transfers to a working fluid. To improve the performance of STs, several studies have been carried out by investigating the geometry [5], using nanofluids [6], vortex generators [7], and Phase Change Materials (PCM) [8]. PVs could only convert a portion of received solar radiation (in the visible range) into electricity, while the rest share of the absorbed energy only increases the PV cells temperature, leading to a reduction in electrical performance and lifetime of PV cells [2]. To resolve the problem and extract the extra absorbed energy by PVs, a combination of PV and ST systems is introduced, named PhotoVoltaic Thermal (PVT) modules [9]. By employing PVTs, both heat and electricity could be produced simultaneously. However, there are still some limitations to the widespread use of PVT systems. One of the major drawbacks of these systems is their low outlet temperature and thermal exergy compared to the STs. To improve the exergy of these systems, different methods such as employing nanofluids, Nano-Phase Change Materials (NPCM), and glass cover are recommended [10]. Many researchers have attempted to increase the performance of PVTs using different enhancement methods like adding nanoparticles to working fluid [11], using PCM [12], NPCM [13], implementing inserts through the working fluid path [14], and employing thermoelectric [15].

Recently, a combination of PVT and ST systems, called PVT-ST, has been introduced to make higher thermal energy. For the first time, the PVT-ST was proposed by *Ma et al*. [16]. They discussed the system's performance under the Shanghai weather for an entire year using 2D numerical modeling. They presented the monthly average thermal and electrical efficiency, where the maximum and minimum electrical power were obtained in July and November, equal to about 35.8 and 18.20 kWh, respectively. Regarding thermal power, the maximum and minimum values were reported for July (35.8 kWh) and January (18.20 kWh), respectively. Using the same 2D numerical model and considering the Mashhad, Iran, weather for one day, *Li et al*. [17] studied the energy and exergy performance of a PVT-ST once the system is covered with and without a glass cover. They showed that the system with a glass cover had higher thermal energy and exergy, while it had lower electrical power in comparison with the unglazed one.

In fixed operating conditions, *Han et al*. [18] examined the performance of PV-ST and PVT-ST systems, numerically. In the former system, the PV system produced only electricity, and the latter provided thermal power. The PVT-ST system reflected better performance at higher solar radiation and ambient temperature in comparison to the PV-ST system. By considering one day in July in Shanghai, *Kazemian et al*. [19] numerically compared the ST, PV, PVT, and PVT-ST systems and scrutinized the impacts of several parameters on the PVT-ST performance. The parameters were working fluid mass flow rate, ambient temperature, solar irradiation, working fluid inlet temperature, and wind speed. They only considered the laminar regime and showed that after solar radiation and working fluid inlet temperature, the mass flow rate was the influential factor on the system performance. In experimental and numerical work, *Chandan et al*. [20] studied the effects of employing glass cover on the PVT-ST system. They reported that utilizing a glass could raise the outlet temperature by about 2-3 °C once the PVT-ST system is employed instead of PVT. However, the electrical power of the glazed PVT-ST was 23% lower than the unglazed one. This study was conducted in Chennai, India, for one day in February.

Based on the literature review, the yearly performance of using PVT-ST has not been investigated in hot and dry climates. Therefore, there is a research gap that should be filled by analyzing the potential use of PVT-ST systems in different cities with such weather. Furthermore, previous studies were only focused on the laminar flow regime, and there is no study on the turbulent one. Consequently, a numerical

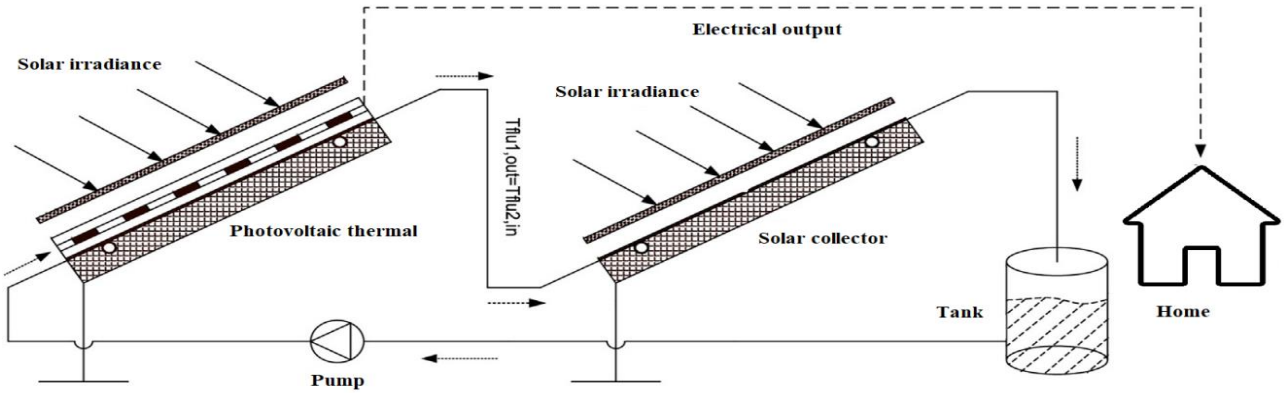

Fig. 1: Diagram of PVT-ST module

model is developed to assess the system's annual performance in terms of the first and second laws of thermodynamics. Four cities—Tehran, Abadan, Baghdad, and Basra—are chosen for this study due to favorable weather conditions (suitable solar radiation throughout the year) for solar systems. In summary, the novelty and goals of the present study are as follows:

- Investigating the performance of the PVT-ST system in six months, including January, March, May, July, September, and November, considering both energy and exergy analyses.
- Comparing the performance of the PVT-ST with common solar systems of single PVT and single ST.
- Examining the performance of the system in four selected cities in six considered months.
- Investigating the impacts of using laminar and turbulent regimes on the performance of these systems for the first time.

The results of this study can get a better insight into the widespread usage of the PVT-ST systems in areas with hot weather.

THEORETICAL SECTION

PVT-ST Physical Model

Fig. 1 shows a PVT-ST diagram in order to simultaneously provide the required electricity and thermal energy for a residential unit. As can be seen, the PVT-ST comprises two separate parts of PVT and ST that are connected with a pipeline. The PVT system consists of different layers, including, from top to bottom, glass cover, PV panel, absorber plate, tubes, and insulation. The ST system includes a glass on top of the absorber plate to increase solar absorption, an absorber plate, tubes, and insulation. The solar collector is made up of copper with serpentine pipes. The geometrical and thermophysical properties of each part are given in Table 1.

As mentioned earlier, a working fluid flow in the thermal collector is utilized beneath the PV cells to reduce the temperature of the PV cells and use extra heat from the system. However, the outlet temperature of the working fluid is not appropriate for many applications. Therefore, the preheated working fluid enters the ST section to increase to the appropriate level.

Mathematical Modeling

A one-dimensional model is developed in the FORTRAN language by means of the TDMA scheme [22, 23] for the discretization to evaluate the performance of the PVT-ST system. It should be mentioned that FORTRAN maintains its outstanding performance and is appealing to scientists due to its great features such as array-oriented design, advanced array support, low execution cost, simplicity of use, robust static guarantees, productivity, and portability [24, 25]. The flowchart of the simulation algorithm is displayed in Fig. 2. It should be mentioned that for the simulation of the ST part, the terms in equations related to the PV surface are removed. Moreover, the outlet temperature of the PVT module is set as the inlet temperature of the ST system.

To model the hybrid system, some assumptions are made, including (1) working fluid flow inside the tubes is assumed to be incompressible and uniform; (2) different layers of both PVT and ST systems have temperature-independent properties and uniform temperature; (3) all surfaces of both systems are assumed to be clean with no dust; (4) expect the glass top surface, other sides of the system are assumed to be completely insulated.

Table 1: The geometrical and thermophysical specifications of the hybrid PVT-ST components [21]

Parameter	Symbol	Value	Unit
Glass cover			
Thickness	δ_g	0.003	m
Length	L	0.63	m
Width	W	0.54	m
Density	ρ_g	2200	$\frac{kg}{m^3}$
Specific heat	$c_{p,g}$	480	$\frac{J}{kg.K}$
Thermal conductivity	k_g	1.1	$\frac{W}{m.K}$
Absorptivity	α_g	0.05	-
Emissivity	ϵ_g	0.92	-
Transmissivity	τ_g	0.936	-
Absorber plate and tubes (copper)			
Thickness of absorber	δ_{ab}	0.0003	m
Thickness of tube	δ_t	0.001	m
Outer diameter of tube	d_t	0.008	m
Length	L	0.63	m
Width	W	0.54	m
Density	$\rho_{ab/t}$	8920	$\frac{kg}{m^3}$
Specific heat	$c_{p,ab/t}$	385	$\frac{J}{kg.K}$
Thermal conductivity	$k_{ab/t}$	398	$\frac{W}{m.K}$
Absorptivity	$\alpha_{ab/t}$	0.95	-
Emissivity	$\epsilon_{ab/t}$	0.88	-
PV panel			
Thickness	δ_{pv}	0.0003	m
Length	L	0.63	m
Width	W	0.54	m
Density	ρ_{pv}	2330	$\frac{kg}{m^3}$
Specific heat	$c_{p,pv}$	700	$\frac{J}{kg.K}$
Thermal conductivity	k_{pv}	84	$\frac{W}{m.K}$
Absorptivity	α_{pv}	0.93	-
Reference temperature coefficient	β_{pv}	0.0045	-
Packing factor	r_{pv}	0.94	$\frac{1}{K}$
Reference PV cell efficiency	η_{pv}	0.016	-
Storage tank			
Volume	V	2	m^3

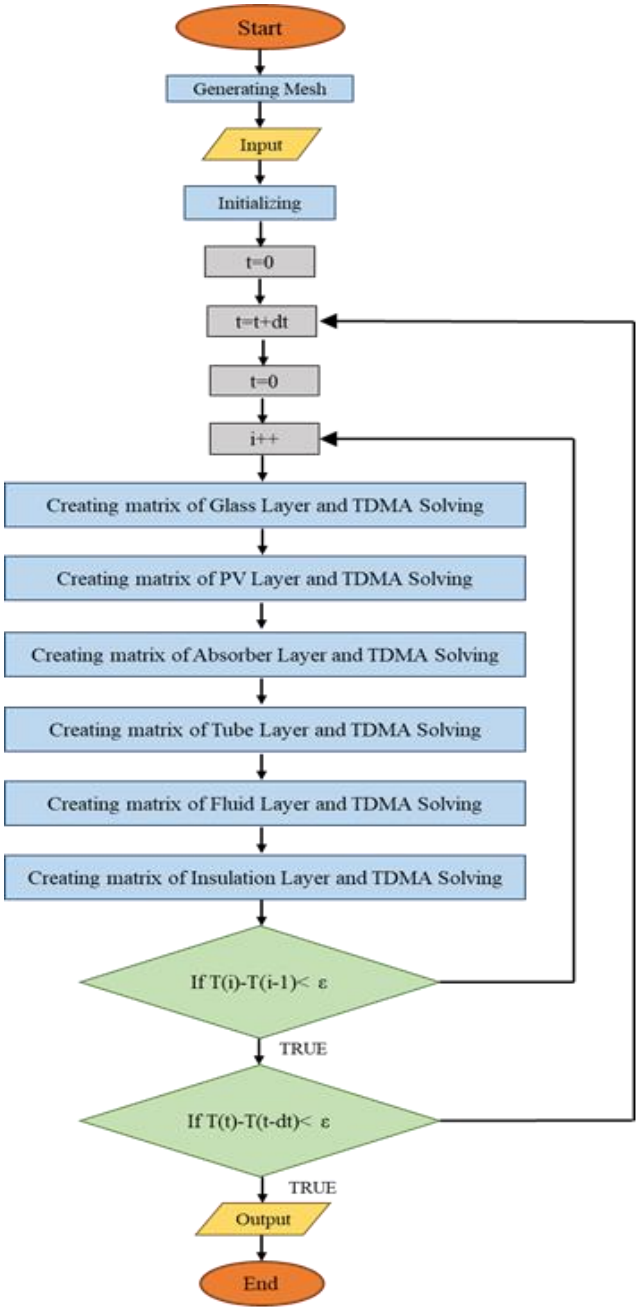

Fig. 2 Flowchart of simulation algorithm used for PVT-ST system modeling

The following governing equations are solved simultaneously. The energy equation for glass cover is:

$$(\rho\ \ \delta\ \ c_p)_g \frac{dT_g}{dt} = \alpha_g G - h_{rad,g\to amb}\left(T_g - T_{sky}\right) - h_{wind}\left(T_g - T_{amb}\right) + U_{cond,g\to pv}\left(T_{pv} - T_g\right) + \delta_g \nabla.\left(k_g \nabla T_g\right) \quad (1)$$

$\alpha_g G$ is the share of the solar irradiation absorbed by the glass cover, and the second and third terms refer to the convective and radiative heat transfer to the surrounding ambient. In this equation, ρ, T, δ, α, G, and c_p are density, temperature, thickness, absorptivity, solar radiation, and specific heat capacity, respectively. The subscripts of g, pv, and amb refer to glass cover, PV panel, and ambient. T_{sky} presents the sky temperature calculated by Eq. (2) [26], which is employed for calculating the heat transfer coefficient of radiation (Eq. (3)):

$$T_{sky} = 0.0552 {T_{amb}}^{1.5} \quad (2)$$

$$h_{rad,g\to amb} = \varepsilon_g \sigma \left({T_g}^2 + {T_{sky}}^2\right)\left(T_g + T_{sky}\right) \quad (3)$$

Herein, ε and σ present emissivity and Stefan Boltzman constant (5.67 10^{-8} W/m^2 K^4), respectively. Moreover, in Eq. (1), h_{wind} and $U_{cond,g\to pv}$ present the convection heat transfer coefficient related to the wind speed on the flat plate (V_{wind}) and overall heat transfer coefficient between the PV panel and glass, respectively, defined as:

$$h_{wind} = \begin{cases} 5.7 + 3.8 V_{wind},\ V_{wind} < 5\ \dfrac{m}{s} \\ 6.47 + {V_{wind}}^{0.78},\ V_{wind} \geq 5\ \dfrac{m}{s} \end{cases} \quad (4)$$

$$U_{cond,g\to pv} = \frac{1}{\frac{\delta_g}{2k_g} + \frac{\delta_{pv}}{2k_{pv}} + R''_{g\to pv}} \quad (5)$$

Herein, k and $R''_{g\to pv}$ present the thermal conductivity coefficient and the thermal resistance among the glass and PV surface per unit area.

To write the energy conversion equation for the PV layer, the absorbed share of solar irradiation passed from the glass cover ($\alpha_{pv}\tau_g G$), the electrical power generated in cells (E_{el}), and the conduction with other layers should be considered as follow:

$$(\rho\ \ \delta\ \ c_p)_{pv} \frac{dT_{pv}}{dt} = \alpha_{pv}\tau_g G - U_{cond,pv\to ab}\left(T_{pv} - T_{ab}\right) - U_{cond,g\to pv}\left(T_{pv} - T_g\right) - E_{el} + \delta_{pv} \nabla.\left(k_{pv} \nabla T_{pv}\right) \quad (6)$$

Where, α_{pv} and τ_g are the absorptance and transmittance of the PV panel and glass cover, respectively. Moreover, $U_{cond,pv\to ab}$ presents the overall heat transfer coefficient between the two layers of PV and absorber, which can be determined in the same way like $U_{cond,g\to pv}$. E_{el} is generated electricity per unit area calculated from [27]:

$$E_{el} = -K_1\beta_{pv}T_{pv} + K_2 \quad (7)$$

$$K_1=\tau_g G\eta_{0,pv}r_{pv} \quad \& \quad K_2=K_1\left(1+298\beta_{pv}\right)$$

$$K_1=\tau_g G\eta_{0,pv}r_{pv} \quad \& \quad K_2=K_1\left(1+298\beta_{pv}\right)$$

β_{pv}, r_{pv}, and $\eta_{0,pv}$ are some constant coefficients related to the type of PV listed in Table 1.

The energy equation for the absorber plate is as follows:

$$(\rho\ \ \delta\ \ c_p)_{ab}\frac{dT_{ab}}{dt} = U_{cond,pv\to ab}\left(T_{pv}-T_{ab}\right)-\frac{A_{ab,t}}{A_{ab}}U_{cond,ab\to t}(T_{ab}-T_t) \quad (8)$$

$$(\rho\ \ \delta\ \ c_p)_{ab}\frac{dT_{ab}}{dt} = U_{cond,pv\to ab}\left(T_{pv}-T_{ab}\right)-\frac{A_{ab,t}}{A_{ab}}U_{cond,ab\to t}(T_{ab}-T_t)$$

$$-\frac{A_{ab,in}}{A_{ab}}U_{cond,ab\to in}(T_{ab}-T_{in})+\delta_{ab}\nabla.(k_{ab}\nabla T_{ab})$$

In this equation, the t, ab, and in, in order, refer to the tube, absorber plate, and insulation. A refers to the computational surface area, and $U_{cond,ab\to t}$ and $U_{cond,ab\to in}$ present the overall heat transfer coefficients between the absorber and two other parts, namely, tube and insulation, respectively, which can be determined using a similar equation as Eq. (5).

Next, the energy equation for the tube wall:

$$(\rho\ \ \delta\ \ c_p)_t Pdx\frac{dT_t}{dt} = A_{ab,t}U_{cond,ab\to t}(T_{ab}-T_t)+A_{in,t}U_{cond,t\to in}(T_{in}-T_t) \quad (9)$$

$$(\rho\ \ \delta\ \ c_p)_t Pdx\frac{dT_t}{dt} = A_{ab,t}U_{cond,ab\to t}(T_{ab}-T_t)+A_{in,t}U_{cond,t\to in}(T_{in}-T_t)$$

$$+h_{conv,t\to f}Pdx\left(T_f-T_t\right)+k_t\delta_t Pdx\frac{\partial^2 T_t}{\partial x^2}$$

Where, $U_{cond,t\to in}$ and $h_{conv,t\to f}$ stand for the overall heat transfer coefficient between the tube and insulation and convective heat transfer coefficient (subscript of f refers to fluid), respectively.

Finally, the energy equation for the working fluid is:

$$(\rho\ \ A\ \ c_p)_f dx\frac{dT_f}{dt} = h_{conv,t\to f}Pdx\left(T_t-T_f\right) - \dot{m}_f c_{p,f}dx\frac{\partial T_f}{\partial x}+\frac{\partial}{\partial x}\left(k_f A_f\frac{\partial T_f}{\partial x}\right)dx \quad (10)$$

$$(\rho\ \ A\ \ c_p)_f dx\frac{dT_f}{dt} = h_{conv,t\to f}Pdx\left(T_t-T_f\right) - \dot{m}_f c_{p,f}dx\frac{\partial T_f}{\partial x}+\frac{\partial}{\partial x}\left(k_f A_f\frac{\partial T_f}{\partial x}\right)dx$$

To calculate the convection heat transfer ($h_{conv,t\to f}$), the Nusselt number (Nu) can be used as follow:

$$h_{conv,f\to t} = \frac{Nu_f k_f}{d_t} \quad (11)$$

where $d_t$stands for the inner tube diameter. The Nu number calculation in the circular tube depends on the flow regime, where for the laminar and turbulent regimes, respectively, Eqs. (12) and (13) can be used [28-30]:

$$Nu_f = 4.36+\frac{0.086\left(\frac{Re_f\ Pr_f\ d_t}{L_t}\right)^{1.33}}{1+Pr_f\left(\frac{Re_f\ d_t}{L_t}\right)^{0.83}} \quad (12)$$

$$Nu_f = \frac{\left(\frac{f}{8}\right)(Re_f-1000)Pr_f}{1+12.7\left(\frac{f}{8}\right)^{1/2}\left(Pr_f^{\ 2/3}-1\right)} \quad (13)$$

Where, in Eq. (12), L_t is the length of the tube, and, in Eq. (13), f is the friction factor determined by the following equation for turbulent regime [31]:

$$f = \frac{1}{(0.79\,ln(Re_f)-1.64)^2} \quad (14)$$

Two dimensionless numbers of Reynolds (Re) and Prandtl (Pr) in Eq. (12) and (13) are determined using the following equations [32]:

$$Re_f = \frac{4\dot{m}_f}{\pi d_t\mu_f} \quad (15)$$

$$Pr_f = \frac{\mu_f c_{p,f}}{k_f} \quad (16)$$

Where, $\dot{m}_f$ and μ_f are the mass flow rate and dynamic viscosity of the working fluid, respectively. It is mentioned that the adiabatic boundary condition is set to the tube wall and absorber plate, i.e., the $U_{cond,t\to in}$ and $U_{cond,t\to in}$ are assumed to be 0 in this study. Moreover, temperature and mass flow rate are applied for the boundary condition of the inlet of the tube, while for the outlet, the zero gradients for the temperature variable are set.

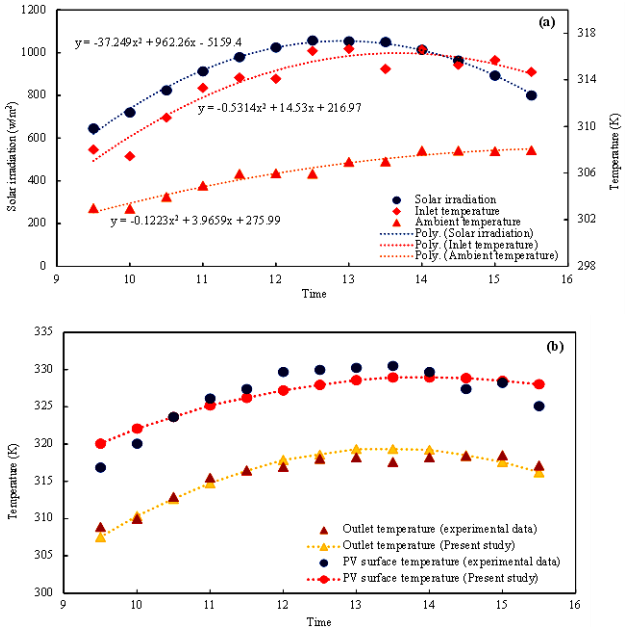

Fig. 3: (a) weather conditions of Mashhad and (b) temporal variations of the temperatures of working fluid outlet and PV surface obtained in this study and experiments conducted by Maadi et al. [21]

Performance analysis

The PVT-ST performance is assessed from the energy and exergy viewpoints. As discussed earlier, this system is capable of producing thermal and electrical power simultaneously. Therefore, the thermal and electrical power is calculated as:

$$E_{th}^{''} = \dot{m}_f c_{p,f}(T_{outlet,f}-T_{inlet,f}) \quad (17)$$

$$E_{el}^{''} = E_{el} A_{pvt} \quad (18)$$

Where, A_{pvt} and E_{el} are the surface area of the PVT system and electrical power per area calculated by Eq. (7). Moreover, the thermal and electrical efficiencies of this system are as follows [9, 33]:

$$\eta_{th} = \frac{E_{th}^{''}}{E_{in}^{''}} = \frac{\dot{m}_f c_{p,f}(T_{outlet,f}-T_{inlet,f})}{(\alpha_{pv}+\alpha_{ab})\tau_g G A_{total}} \quad (19)$$

$$\eta_{el} = \frac{E_{el}^{''}}{E_{in}^{''}} = \frac{E_{el}}{\alpha_{pv}\tau_g G} \quad (20)$$

Where, A_{total} is the total area covered by PVT and ST systems.

The exergy balance for the PVT-ST system is written as [34]:

$$Ex_{in}^{''} = Ex_{inlet}^{''} - Ex_{outlet}^{''} + Ex_{el}^{''} + Ex_{loss}^{''} \quad (21)$$

Herein, $\dot{E}x''_{in}$ presents the value of the solar irradiation exergy received by the total surface of the PVT-ST system (A_{total}), calculated by [35, 36]:

$$Ex_{in}^{''} = GA_{total}\left(1 - \frac{4T_{amb}}{3T_{sun}} + \frac{1}{3}\left(\frac{T_{amb}}{T_{sun}}\right)^4\right) \quad (22)$$

Were T_{sun} is the sun's surface temperature and is equal to 5800 K [37]. The first and second terms on the right-hand side of Eq. (21) refer to the thermal exergy [12]:

$$Ex_{in}^{''} = E_{th}^{''} - \dot{m}_f c_{p,f} T_{amb}\, ln\left(\frac{T_{outlet}}{T_{inlet}}\right) \quad (23)$$

Furthermore, electrical exergy is equivalent to electrical energy; therefore, its value is [37]:

$$Ex_{el}^{''} = E_{el}^{''} \quad (24)$$

Therefore, both thermal and electrical efficiencies, respectively, are defined as:

$$\eta_{II,th} = \frac{Ex_{th}^{''}}{Ex_{in}^{''}} \quad (25)$$

$$\eta_{II,el} = \frac{Ex_{el}^{''}}{Ex_{in}^{''}} \quad (26)$$

Validation

The one-dimensional model's validity is evaluated by the experimental data provided by *Maadi et al.* [21]. They investigated the PVT performance under the Mashhad (Iran, with a latitude of 36° and a longitude of 59°) weather conditions between 9:30 AM and 3:30 PM, as shown in Fig. 3(a). In this Fig, the experimental data with their corresponding fitted curves are shown. The dimensions of their system were similar to the dimensions of the PVT part used in the present study. Moreover, the mass flow rate of the working fluid was 0.00834 kg/s. Fig. 3 illustrates the temporal variations of temperatures of the working fluid outlet and PV surface obtained by the present model and experimental data reported by *Maadi et al.* [21]. The Figiure shows a satisfactory agreement between the results, where for working fluid outlet and PV surface temperatures, the average error is around 2% and 1.8%, respectively. Besides the uncertainty in experiments, using the one-dimensional model and applying some assumptions in this simulation may lead to these differences.

RESULTS AND DISCUSSION

The main objective of this study is to evaluate the feasibility of using PVT-ST in different cities with hot weather conditions, as discussed in the first section. Next, the hourly performance of the system is studied for the weather conditions of Tehran. Then, a comparative study is done to assess the hybrid system performance alongside the single typical ST and PVT modules. This study is carried out under different working fluid mass flow rates ($\dot{m}_f$) as one of the critical operating conditions. Next, regarding the optimum $\dot{m}_f$, the monthly performance of the PVT-ST system is studied under weather conditions in four cities of Tehran, Abadan, Baghdad, and Basra. We considered six months of a year to represent various weather conditions around an entire year.

Weather conditions of different cities

Fig. 4 shows the temporal variations of the solar irradiation, ambient temperature, and wind speed in January, March, May, July, September, and November for four cities of Tehran, Abadan, Baghdad, and Basra. These six months are selected to examine the yearly performance of the PVT-ST system as representative months of a year. All these cities have hot weather and are suitable for using solar systems. In particular, the climate of Tehran can be described as hot and dry in summer, mild in spring and autumn, and cold and wet in winter. However, based on the Köppen climate classification BWh, Abadan, Baghdad, and Basra have hot subtropical desert, hot desert, and desert climates, respectively. The hottest and coldest months with maximum and minimum solar radiation are July and January, respectively. However, each city's solar heat flux, ambient temperature, and wind speed vary. For example, in July, Tehran has the lowest, and Abadan possesses the highest ambient temperature among all cities. Moreover, the wind speed is higher in Basra compared to other cities, leading to a higher heat loss to the ambient surrounding. It's worth noting that the inlet temperature is assumed to be the same as the ambient temperature in all experiments.

Hourly performance investigation of PVT-ST system under laminar and turbulent regimes

To understand the thermal and electrical behavior of the PVT-ST, the produced power on a typical day in July in Tehran is investigated. For this purpose, first, the hourly variations of the temperatures of the working fluid and PV panel are discussed. Considering laminar and turbulent regimes, the results are presented in Fig. 5 for the different mass flow rates. Therefore, for the laminar regime, three $\dot{m}_f$ of 0.00394, 0.00788, and 0.01182 kg/s, and for the turbulent regime, 0.02252, 0.02646, and 0.0304 kg/s are considered.

According to Fig. 5(a), the outlet temperature rises to the maximum at around 11:00 AM for all mass flow rates when the system receives a higher amount of solar radiation, as shown in Fig. 4 for Tehran. Moreover, the mass flow rate in the laminar regime possesses a higher outlet temperature than the turbulent one. Setting 11:00 AM as the basis of comparison, using a $\dot{m}_f$ = 0.00394 kg/s provides an outlet temperature of around 333.16 K, which decreases to 319.1 K (with a 4.2% reduction) at $\dot{m}_f$ = 0.01182 kg/s. Using turbulent flow reduces the outlet temperature even more; however, rising $\dot{m}_f$ from 0.02252 to 0.0304 kg/s, the outlet temperature at 11:00 AM is reduced by only 0.4%. This shows that the effect of mass flow rate on the outlet temperature decreases by rising the mass flow rate, particularly in a turbulent regime. The reason for this reduction in outlet temperature by raising the $\dot{m}_f$ is due to the reduction in working fluid residence time in the tube, and as a result, absorbing more heat. Despite the lower outlet temperature, the quantity of absorption rate of heat is greater at higher working fluid mass flows. In other words, the higher heat transfer coefficient at high $\dot{m}_f$ leads to absorbing more heat from the PV cells. For example, the highest PV temperature belongs to the system with the $\dot{m}_f$ = 0.00394 kg/s (turbulent flow), while using $\dot{m}_f$ = 0.0304 kg/s (turbulent flow) can reduce the PV temperature by nearly 7.5 K. It is interesting to point out that similar to the effects of $\dot{m}_f$ on outlet temperature, the PV temperature reduction is more pronounced in the laminar regime.

Fig. 6(a) displays the hourly generated power per area of the PVT-ST at various mass flow rates in July. Although the outlet temperature grows by reducing the $\dot{m}_f$ and the laminar regime possesses a higher outlet temperature, the thermal power significantly rises by increasing $\dot{m}_f$. This is because of the considerable improvement in the convective heat transfer coefficient in the working fluid by increasing the mass flow rate. This variation is higher in the laminar

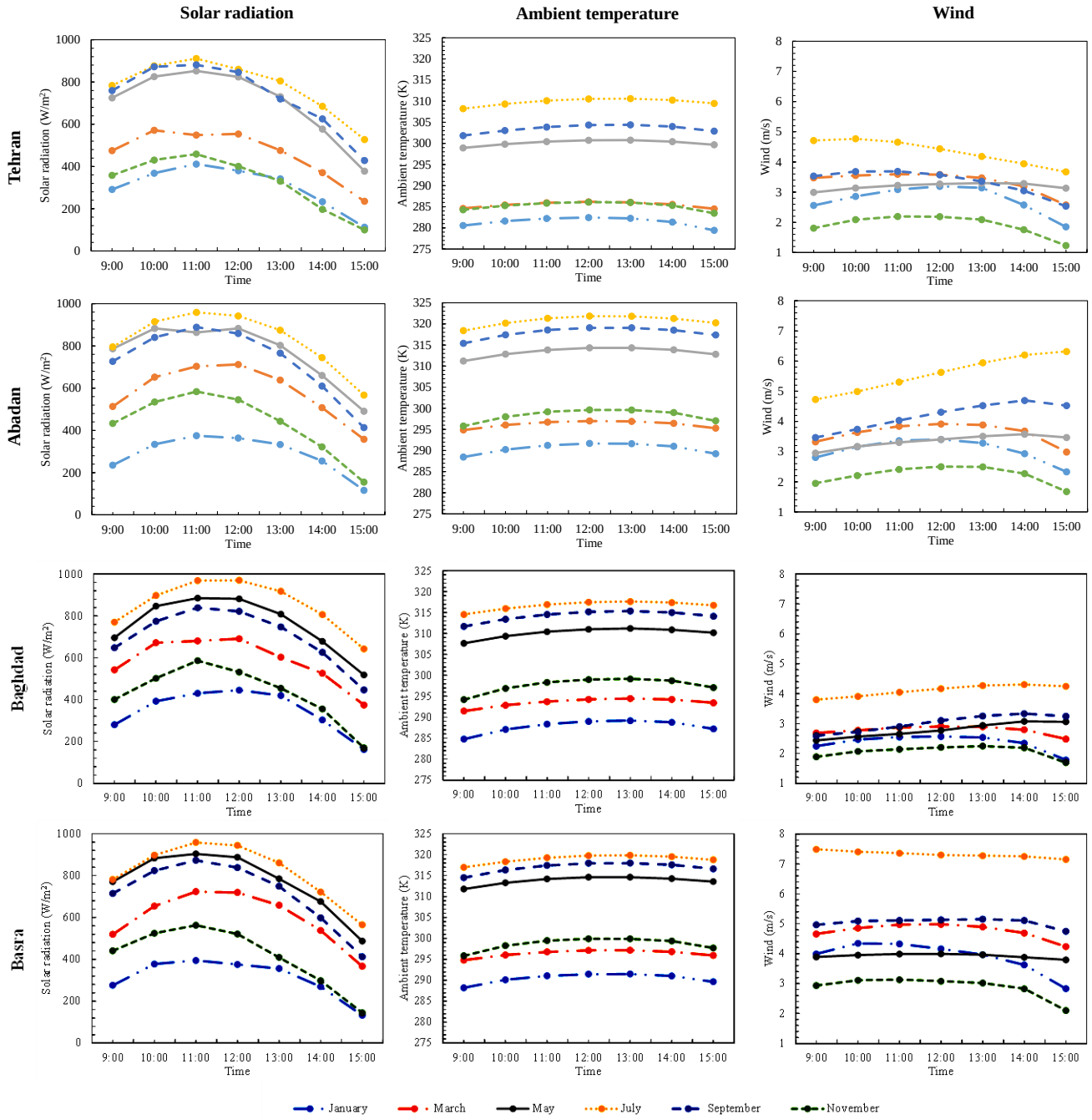

Fig. 4: Variations of the solar irradiation, ambient temperature, and wind speed in January, March, May, July, September, and November for four Cities of Tehran, Abadan, Baghdad, and Basra

regime, though for the turbulent regime, the rise in mass flow rate slightly increases the thermal power. Moreover, the Fig shows that increasing the solar radiation rises the thermal power produced by the system up to around 722 W/m^2 at 11:00 AM at the highest considered $\dot{m}_f$. At this time, the thermal power is 558 W/m^2 for 0.00394 kg/s.

The produced electrical power is a direct function of two variables, solar radiation and PV cell temperature, according to Eq. (7). Increasing the former increases the value of the generated power, whilst increasing the latter decreases the cell's efficiency and, consequently, the amount of generated electricity. Therefore, the system generates

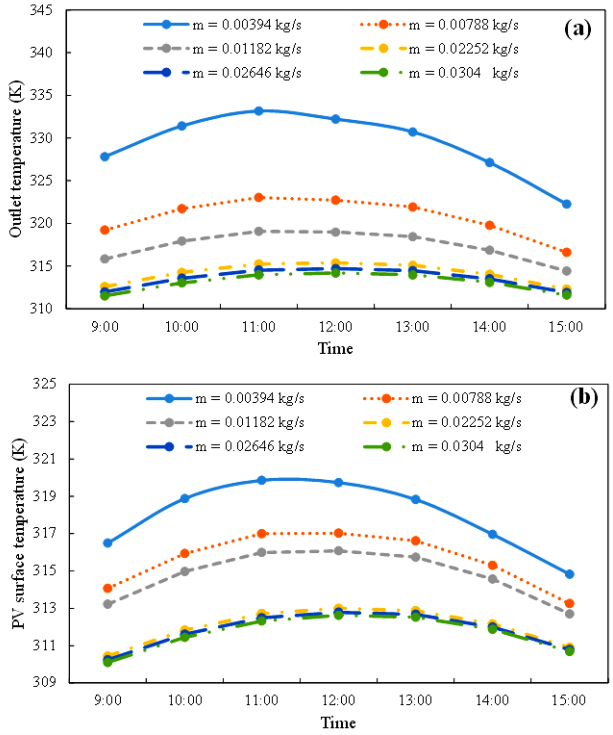

Fig. 5: Hourly variations of the (a) outlet temperature of the working fluid and (b) PV surface temperature at different mass flow rates in July in Tehran

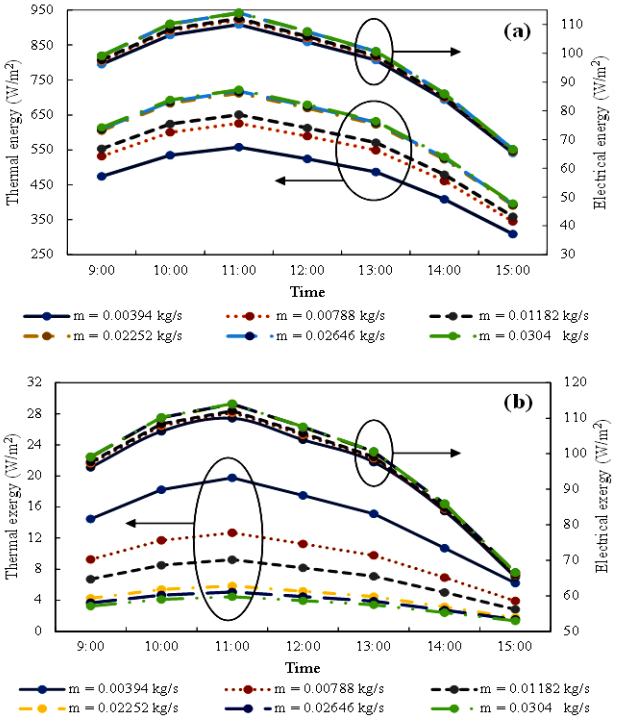

Fig. 6: Hourly variations of the (a) thermal and electrical power per area and (b) thermal and electrical exergy per area of the PVT-ST system at different mass flow rates in July in Tehran

the most electricity at midday, when solar radiation is at its peak. Moreover, compared to the laminar and turbulent regimes, the turbulent regime produces more electricity due to the increased heat harvesting and the decrease in PV temperature. Eventually, the maximum electrical output of 114 W/m^2 is achievable at 11:00 AM in a turbulent regime with $\dot{m}_f$ = 0.0304.

To evaluate the quality of the energy, the exergy is employed as shown in Fig. 6(b) in July in Tehran for two considered regimes. Because the whole of the electrical power represents valuable energy, the Fig demonstrates that an analogous trend can be seen for electrical exergy in comparison to electrical power. As a direct consequence of this, the electrical exergy of the system is equivalent to its electrical power. In contrast, the thermal exergy dramatically reduces compared to the thermal power, especially in a turbulent regime. In other words, the thermal exergy shows a lower value because of the lesser outlet temperature, as revealed in Fig. 5(a) in the turbulent regime. For example, considering 11:00 AM, the system thermal exergy is decreased from 19.8 to 4.5 W/m^2 once the $\dot{m}_f$ changes from 0.00394 to 0.0304 kg/s.

Potential of using PVT-ST instead of single typical ST and PVT systems

The performance of the PVT-ST is compared with the commonly used single ST and PVT under the same and fixed conditions of Tehran weather in July. The only variable parameter is the water mass flow rate, which is set in a way that both laminar ($\dot{m}_f$ = 0.00394, 0.00788, and 0.01182 kg/s) and turbulent ($\dot{m}_f$ = 0.02252, 0.02646, and 0.0304 kg/s) regime can be investigated.

Fig. 7 shows the average thermal power per area and thermal efficiency of considered systems at different mass flow rates. Regardless of system type, increasing $\dot{m}_f$ improves the thermal performance of the solar system due to the growth in the convective heat transfer coefficient throughout the tube. This increment is more pronounced at lower mass flow rates in the laminar regime, e.g., rising $\dot{m}_f$ from 0.00394 to 0.00788 kg/s leads to an around 14.2% improvement in thermal power in the ST system. After that, the Fig experiences a relatively noticeable rise once the regime changes from laminar to turbulent. However, the variation of thermal power with the $\dot{m}_f$ is slight in the turbulent regime. Eventually, the maximum thermal power per area can be achieved at $\dot{m}_f$ = 0.0304 kg/s in the turbulent regime.

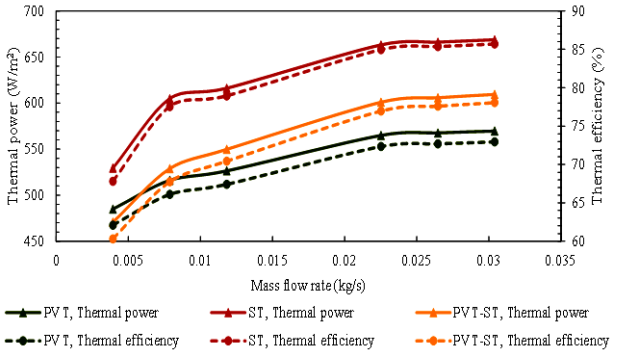

Fig. 2: Comparing the average thermal power per area and thermal efficiency of PVT, ST, and PVT-ST systems at different mass flow rates on a typical day in Tehran in July

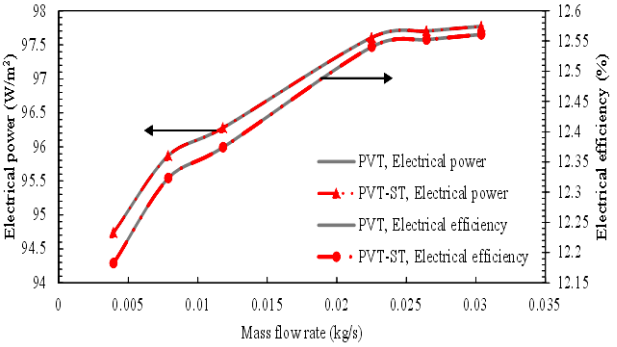

Fig. 8: Comparing the average electrical power per area and electrical efficiency of the single PVT and PVT-ST modules at different mass flow rates in Tehran in July

Comparing the thermal power of the three mentioned systems, the ST system produces the highest thermal power per area at all considered mass flow rates. The primary reasons which contribute to this result are, first, that, in contrast to other systems, the ST system turns all of the energy that is absorbed into heat, and second, that the absorber plate has a higher absorption coefficient than the PV surface. The average thermal power per area of the ST system is varied between 529.4 and 668.8 W/m^2, respectively, for 0.00394 (laminar regime) and 0.0304 kg/s (turbulent regime). The results demonstrate that the thermal power of the PVT system is less affected by the mass flow rate compared to the two other systems. Moreover, expect $\dot{m}_f$ = 0.00394 kg/s where the PVT thermal power is higher than that of the PVT-ST system, in all mass flow rates, the PVT-ST system reflects better performance. For example, the PVT-ST system can produce 40 W per area more thermal in comparison with the single PVT module. In terms of thermal efficiency, the ST module has the best performance, where the optimum thermal efficiency can be obtained at $\dot{m}_f$ = 0.0304 kg/s and equal to 85.7%. This is followed by the thermal performance of PVT-ST and PVT systems with 78% and 72.9%, respectively.

Although the ST collector has the ability to produce the highest amount of thermal power, the main drawback of this system is its disability to generate electricity. The electrical power and efficiency of the PVT and PVT-ST systems are plotted for different mass flow rates in Fig. 8. It should be mentioned that due to considering an equal surface area for PV surfaces of the two systems, both systems illustrate the same amount of electrical power per area. Increasing the mass flow rate enhances the amount of extracted heat from the PV surface, leading to a reduction in PV cells. Accordingly, according to Eqs. (7), (18), and (20), by decreasing the PV cells temperature, the electrical power and, in turn, the electrical efficiency of the cells enhances. Setting the 0.00394 kg/s as the basis of comparison, increasing the mass flow rate results in an escalation in electrical power by 1.2%, 1.6%, 3%, 3.1%, and 3.2%, respectively, once $\dot{m}_f$ = 0.00788, 0.01182, 0.02252, 0.02646, and 0.0304 kg/s are applied. Consequently, the maximum electrical efficiency can be achieved by using the highest mass flow rate to reach the electrical efficiency of 12.56%.

Finally, the thermal and electrical exergy of the systems is discussed. The exergy analysis is a useful tool to better understand the energy quality. Fig. 9 displays the average thermal and electrical exergy per area for PVT, ST, and PVT-ST systems at different mass flow rates in Tehran in July. According to the Fig, increasing the mass flow rate declines the thermal exergy due to the increment in pressure drop and, in turn, irreversibility. Moreover, the PVT-ST system reflects a performance improvement in terms of thermal exergy followed by ST and PVT ones, respectively, thanks to the significant increment in working outlet temperature. Consequently, the maximum thermal exergy per area is obtained at the lowest $\dot{m}_f$ = 0.00394 kg/s for cases, e.g., the thermal exergy of PVT-ST, ST, and PVT are 14.6, 9.4, and 7.9 W/m^2, respectively. By transitioning from laminar to turbulent, i.e., using $\dot{m}_f$ = 0.0304 kg/s, the thermal exergy of PVT-ST, ST, and PVT systems drop by 77.5%, 78.9%, and 81.8%, respectively.

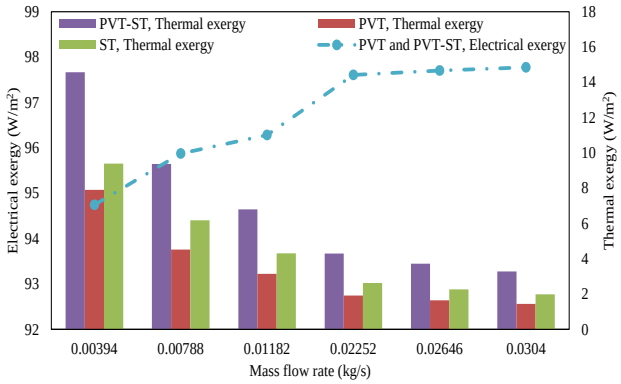

Fig. 9 Variations of the thermal and electrical exergy per area of PVT, ST, and PVT-ST systems at different mass flow rates in Tehran in July

Based on the energy analysis results, the thermal power of the PVT-ST and single PVT is greater than the electrical power, while the reverse result can be seen for the exergy of these systems. In other words, because of the quality of the electrical energy compared to the thermal energy, the electrical exergy per area is higher than the thermal exergy. Furthermore, in contrast to the thermal exergy, the electrical exergy grows by increasing the mass flow rate thanks to the increment in heat transfer coefficient inside the tube in higher mass flow rates, resulting in a reduction in PV surface temperature. From Fig. 9, the average electrical exergy per area of both PVT and PVT-ST is relatively the same, reaching optimum at $\dot{m}_f$ = 0.0304 kg/s with the value of 97.8 W/m^2. It should also be mentioned that the electrical exergy variations with a mass flow rate in the laminar regime are more pronounced than in the turbulent one.

Performance of the PVT-ST in different cities

Finally, the performance of the hybrid system is examined under weather conditions in four cities of Tehran, Abadan, Baghdad, and Basra for six months of a year (for weather conditions, see Fig. 4). It should be mentioned that all four cities have hot climates with high solar radiation and ambient temperature. Furthermore, according to the results for mass flow rate (comparing the laminar and turbulent regimes), $\dot{m}_f$ = 0.0304 kg/s is selected for this section due to its superiority in making higher thermal and electrical power.

First, the outlet temperature of the working fluid is studied and shown in Fig. 10. A similar pattern can be observed for outlet temperature in various cities during different months, where the highest possible outlet temperature can be achieved in July, followed by September and May. Because, according to **Error! Reference source not found.**, the highest levels of solar radiation and ambient temperature can be seen in these months. It is pointed out that the outlet temperature is dependent upon the surrounding temperature, which is assumed as the inlet temperature in the present study. Hence, for instance, in July, Tehran produces a lower outlet temperature due to its lower inlet temperature, while Abadan has a higher outlet temperature because of its higher inlet temperature.

Fig. 11 shows the thermal and electrical power variations v.s time in a day in considered months for (a) Tehran, (b) Abadan, (c) Baghdad, and (d) Basra. Considering the Fig for Tehran, thanks to the higher outlet temperature in July, the maximum thermal power is achieved this month. Moreover, the trend of thermal power is similar to the solar radiation in Fig. 4, peaking at around 11:00 AM. This pattern is relatively repeated in other cities, where the maximum and minimum thermal power can be observed in July and January, respectively. In terms of electrical power, although increasing solar radiation improves the share of electricity production, the PV cell temperature is also increased, leading to decreased electricity generation. However, according to the Fig, the system in all cities can produce maximum electrical power in July.

Finally, to better compare the results, the average thermal power, electrical power, thermal exergy, and electrical exergy for each month in different cities are summarized in Table 2. Moreover, the average of the system performance in six months is also presented. According to this table, there is no significant difference between the power produced in different cities, which shows the potential use of the PVT-ST in four selected cities. The system operating in Basra shows the peak amount of thermal power and exergy with an average of 375.72 and 1.46 W/m^2 during six considered months. Nevertheless, the system generates more electricity (average electrical power and exergy of about 77 W/m^2) in Baghdad as a consequence of higher solar radiation in total during the six months.

Table 2: Average thermal power, electrical power, thermal exergy, and electrical exergy for each month in different cities

	Average value (W/m^2)							
	Parameter	January	March	May	July	September	November	Average of 6 months
Tehran	Thermal power	214.32	365.46	387.41	609.42	391.71	204.36	362.11
	Electrical power	43.75	64.93	96.68	97.77	95.18	45.83	74.02
	Thermal Exergy	0.50	1.35	1.45	3.28	1.46	0.46	1.42
	Electrical exergy	43.75	64.93	96.68	97.77	95.18	45.83	74.02
Abadan	Thermal power	208.05	369.54	413.46	610.44	410.41	221.32	372.20
	Electrical power	39.61	78.28	95.02	98.53	88.26	57.34	76.18
	Thermal Exergy	0.45	1.33	1.58	3.18	1.53	0.51	1.43
	Electrical exergy	39.61	78.28	95.02	98.53	88.26	57.34	76.18
Baghdad	Thermal power	218.02	384.39	399.04	600.71	413.63	139.44	359.21
	Electrical power	48.47	70.85	95.51	103.52	86.37	57.23	76.99
	Thermal Exergy	0.51	1.46	1.49	3.12	1.58	0.20	1.39
	Electrical exergy	48.47	70.85	95.51	103.52	86.37	57.23	76.99
Basra	Thermal power	224.17	379.30	409.53	603.70	419.07	218.56	375.72
	Electrical power	42.95	71.65	95.21	98.25	87.06	55.08	75.03
	Thermal Exergy	0.54	1.41	1.55	3.13	1.61	0.50	1.46
	Electrical exergy	42.95	71.65	95.21	98.25	87.06	55.08	75.03

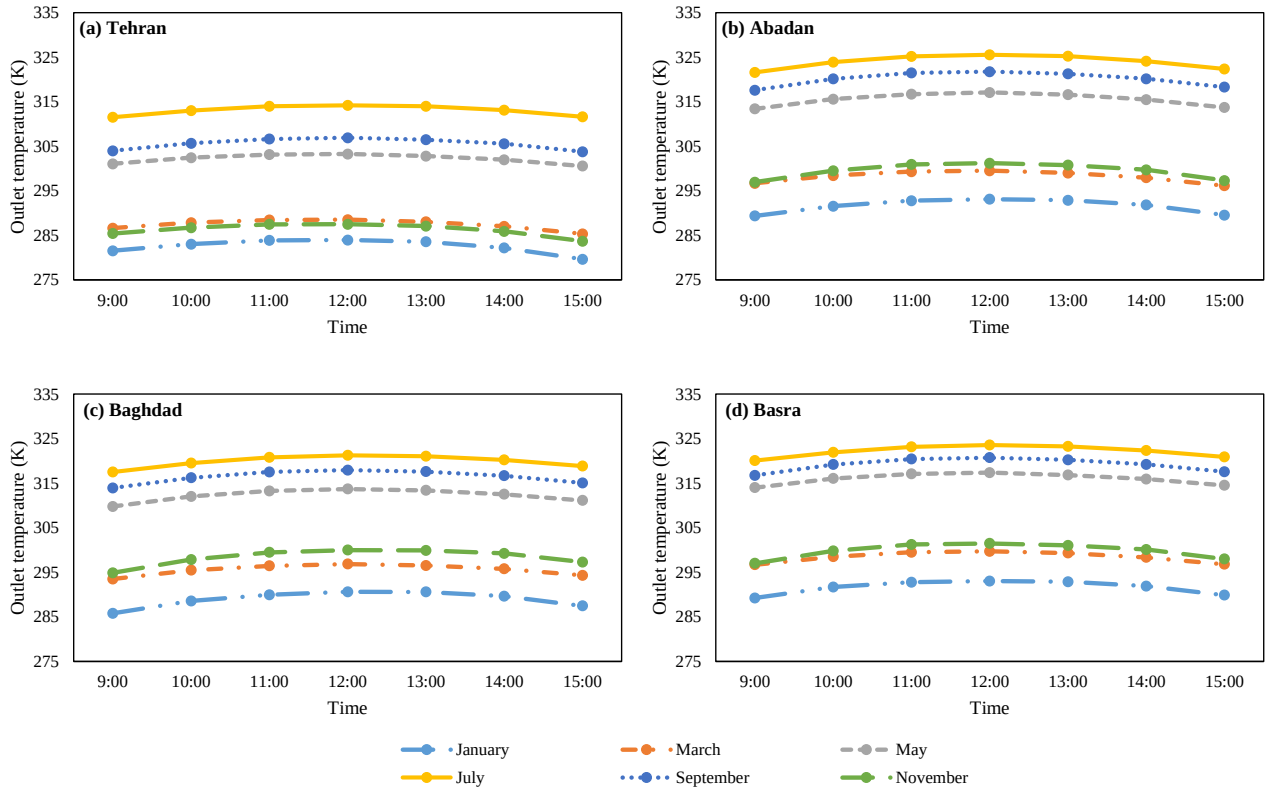

Fig. 3: Variations of the outlet temperature during a day in considered months for (a) Tehran, (b) Abadan, (c) Baghdad, and (d) Basra

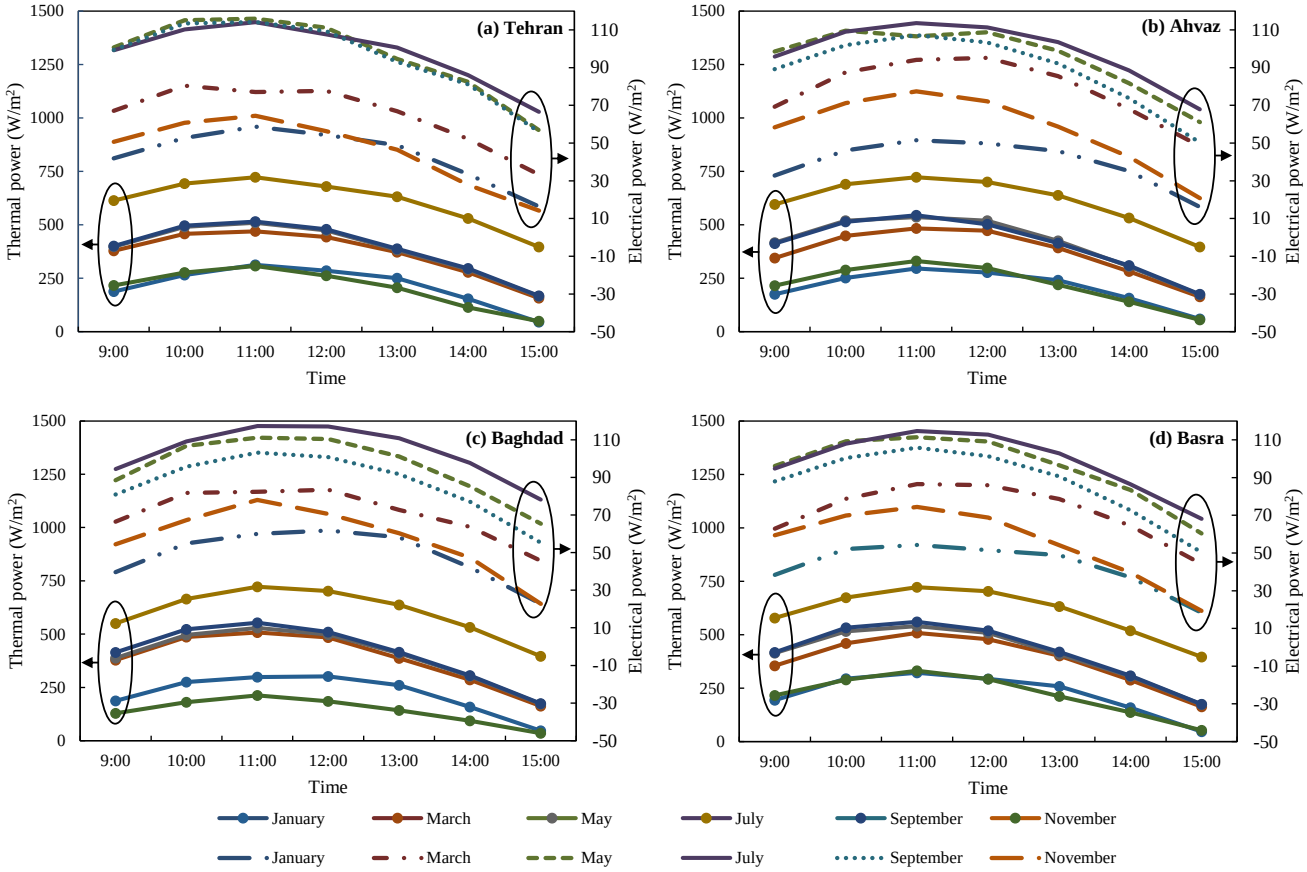

Fig. 4: Variations of the PVT-ST electrical and thermal power per area during a day in considered months for (a) Tehran, (b) Abadan, (c) Baghdad, and (d) Basra

CONCLUSIONS

This numerical study evaluated the potential use of a newly introduced solar system called PVT-ST, which can generate high-temperature thermal energy as well as electricity, simultaneously. For this purpose, the yearly performance of the module in terms of the first and second laws of thermodynamics was investigated in four cities in Iran and Iraq. Furthermore, the influence of the working fluid regime, including laminar and turbulent regimes, on the system performance was scrutinized. Additionally, a comparison was carried out between the PVT-ST and common single PVT and single ST systems. The findings of the present numerical study are:

- In the laminar regime, the outlet temperature was significantly greater than in the turbulent regime. However, as the turbulence regime had a higher heat transfer coefficient, the amount of absorbed energy was higher, leading to a lower PV surface temperature.
- The thermal power significantly rises by increasing the mass flow rate, where, at the highest solar radiation in July in Tehran, the thermal power increased from 558 to 722 W/m^2 by changing the mass flow rate from 0.00394 kg/s (laminar regime) to 0.0304 kg/s (turbulent regime).
- Electrical power and exergy were higher for the turbulent regime due to the harvesting of further heat and decreasing PV surface temperature. However, the thermal exergy is dramatically reduced by raising the mass flow rate due to the lower outlet temperature in the turbulent regime.
- The optimum thermal efficiency was obtained for a single ST system (85.7%) at the highest mass flow rate of 0.0304 kg/s in July, followed by the PVT-ST and PVT systems with 78% and 72.9%, respectively. Moreover, the maximum electrical efficiency was achieved at the highest mass flow rate, equaling 12.56% for both PVT-ST and PVT systems.
- The maximum thermal exergy per area was achieved at the lowest mass flow rate of 0.00394 kg/s for PVT-ST, ST, and PVT, respectively, which showed the superiority of using PVT-ST.

• Monthly performance analysis indicated that Basra had the highest amount of thermal power and exergy with an average of 375.72 and 1.46 W/m^2 during six considered months, while in Baghdad, the system could generate more electricity, an average of 77 W/m^2.

Nomenclature

A	area (m^2)
c_P	specific heat (J/kg.K)
d_t	tube diameter (m)
E	energy (W/m^2)
E''	rate of energy (W)
Ex''	rate of exergy (W)
f	friction factor
G	solar radiation (W/m^2)
h	convective heat transfer (W/m^2 K)
k	thermal conductivity (W/m K)
l	length of tube (m)
$\dot{m}$	mass flow rate (kg/s)
Nu	Nusselt number
Pr	Prandtl number
R''	thermal contact resistance
Re	Reynolds number
r_{PV}	packing factor
t	time (s)
T	temperature (K)
V_{wind}	wind speed (m/s)

Greeks

β_{pv}	reference temperature coefficient
η	efficiency (%)
μ	viscosity (pa s)
α	absorptance
ε	emissivity
τ	transmittance
δ	thickness (m)
ρ	density (kg/m^3)

Subscripts

ab	absorber plate
amb	ambient temperature
$cond$	conduction
$conv$	convection
el	electrical
f	fluid
g	glass cover
in	insulation
out	outlet
th	thermal
pv	photovoltaic module
t	tube

Abbreviation

PV	photovoltaic module
PVT	photovoltaic thermal system
ST	solar thermal
PVT-ST	photovoltaic thermal system with solar thermal collector in series

Received : Dec. 16, 2022 ; Accepted : Apr.24, 2023

REFERENCES

[1] Kazemian A., Khatibi M., Ma T., Peng J., Hongxing Y., A Thermal Performance-Enhancing Strategy of Photovoltaic Thermal Systems by Applying Surface Area Partially Covered by Solar Cells, *Applied Energy*, **329**: 120209 (2023).

[2] Pathak S.K., Sharma P.O., Goel V., Bhattacharyya S., Aybar H.Ş., Meyer J.P., A Detailed Review on the Performance of Photovoltaic/Thermal System Using Various Cooling Methods, *Sustainable Energy Technologies and Assessments*, **51**: 101844 (2022).

[3] Hassan A., Wahab A., Qasim M.A., Janjua M.M., Ali M.A., Ali H.M., Jadoon T.R., Ali E., Raza A., Javaid N., Thermal Management and Uniform Temperature Regulation of Photovoltaic Modules Using Hybrid Phase Change Materials-Nanofluids System, *Renewable Energy*, **145**: 282-293 (2020).

[4] Suman S., Khan M.K., Pathak M., Performance Enhancement of Solar Collectors—A Review, *Renewable and Sustainable Energy Reviews*, **49**: 192-210 (2015).

[5] Zhang D., Tao H., Wang M., Sun Z., Jiang C., Numerical Simulation Investigation on Thermal Performance of Heat Pipe Flat-Plate Solar Collector, *Applied Thermal Engineering*, **118**: 113-126 (2017).

[6] Norouzi N., Bozorgian A., Exergy Performance of a Natural Circulation Solar Collector System Using Aluminum Oxide, Copper, and Copper Oxide Nanofluids, *Iranian Journal of Chemistry and Chemical Engineering (IJCCE)*, **42(3):** 989-1005 (2023).

[7] Sari A., Sadi m., Shafiei Sabet G., Mohammadiun M., Mohammadiun H., Experimental and Numerical Investigation of Implementing a Novel Vortex Generator: A Perforated Delta Wing Vortex Generator (PDWVG) on the Performance of Solar Air Collector, *Iranian Journal of Chemistry and Chemical Engineering (IJCCE),*, **41(9):** 3168-3180 (2022).

[8] Serale G., Goia F., Perino M., Numerical Model and Simulation of a Solar Thermal Collector with Slurry Phase Change Material (PCM) as the Heat Transfer Fluid, *Solar Energy*, **134**: 429-444 (2016).

[9] Maadi S.R., Khatibi M., Ebrahimnia-Bajestan E., Wood D., Coupled Thermal-Optical Numerical Modeling of PV/T Module – Combining CFD Approach and Two-Band Radiation DO Model, *Energy Conversion and Management*, **198**: (2019).

[10] Guedri K., Salem M., Assad M.E.H., Rungamornrat J., Malek Mohsen F., Buswig Y.M., PV/Thermal as Promising Technologies in Buildings: A Comprehensive Review on Exergy Analysis, *Sustainability*,**14(19)**: 12298 (2022).

[11] Sharifpur M., Ahmadi M.H., Rungamornrat J., Malek Mohsen F., Thermal Management of Solar Photovoltaic Cell by Using Single Walled Carbon Nanotube (SWCNT)/Water: Numerical Simulation and Sensitivity Analysis, *Sustainability*, **14(18)**: 11523 (2022).

[12] Kazemian A., Yaser B., Khatibi M., Ma T., Performance Prediction and Optimization of a Photovoltaic Thermal System Integrated with Phase Change Material Using Response Surface Method, *Journal of Cleaner Production*, **290**: 125748 (2021).

[13] Kazemian A., Khatibi M., Maadi S.R., Ma T., Performance Optimization of a Nanofluid-Based Photovoltaic thermal System Integrated with Nano-Enhanced Phase Change Material, *Applied Energy*, **295**: 116859 (2021).

[14] Maadi S.R., Sabzali H., Kolahan A., Wood D., Improving the Performance of PV/T Systems by Using Conical-Leaf Inserts in the Coolant Tubes, *Solar Energy*, **212**: 84-100 (2020).

[15] Kolahan A., Maadi S.R., Kazemian A., Schenone C., Ma T., Semi-3D Transient Simulation of a Nanofluid-Base Photovoltaic Thermal System Integrated with a Thermoelectric Generator, *Energy Conversion and Management*, **220**: 113073 (2020).

[16] Ma T., Li M., Kazemian A., Photovoltaic Thermal Module and Solar Thermal Collector Connected in Series to Produce Electricity and High-Grade Heat Simultaneously, *Applied Energy*, **261**: 114380 (2020).

[17] Li M., Zhong D., Ma T., Kazemian A., Gu W., Photovoltaic Thermal Module and Solar Thermal Collector Connected in Series: Energy and Exergy Analysis, *Energy Conversion and Management*, **206**: 112479 (2020).

[18] Han Z., Liu K., Li G., Zhao X., Shittu S., Electrical and Thermal Performance Comparison between PVT-ST and PV-ST Systems, *Energy*, 121589 (2021).

[19] Kazemian A., Parcheforosh A., Salari A., Ma T., Optimization of a Novel Photovoltaic thermal Module in Series with a Solar Collector Using Taguchi Based Grey Relational Analysis, *Solar Energy*, **215**: 492-507 (2021).

[20] Suresh V., Iqbal S.M., Reddy K., Pesala B., 3-D Numerical Modelling and Experimental Investigation of Coupled Photovoltaic Thermal and Flat Plate Collector, *Solar Energy*, **224**: 195-209 (2021).

[21] Maadi S.R., Kolahan A., Passandideh-Fard M., Sardarabadi M., Moloudi R., Characterization of PVT Systems Equipped with Nanofluids-Based Collector from Entropy Generation, *Energy Conversion and Management*, **150**: 515-531 (2017).

[22] Khatibi M., Kowsari M.M., Golparvar B., Niazmand H., Sharafian A., A Comparative Study to Critically Assess the Designing Criteria for Selecting an Optimal Adsorption heat Exchanger in Cooling Applications, *Applied Thermal Engineering*, **215**: 118960 (2022).

[23] Mahdavikhah M., Khatibi M., Niazmand H., Relative Importance of Inter-Particle Mass Transfer Resistance in the Modeling of Adsorption Chiller Porous Bed, *International Journal of Refrigeration*, **106**: 104-112 (2019).

[24] Mak L., Taheri P., An Automated Tool for Upgrading Fortran Codes, *Software*, **1(3)**: 299-315 (2022).

[25] Kedward L.J., Aradi B., Čertík O., Curcic M., Ehlert S., Engel P., Goswami R., Hirsch M., Lozada-Blanco A., Magnin V., The state of Fortran, *Computing in Science & Engineering*, **24(2)**: 63-72 (2022).

[26] Swinbank W.C., Long-Wave Radiation from Clear Skies, *Quarterly Journal of the Royal Meteorological Society*, **89(381)**: 339-348 (1963).

[27] Skoplaki E., Palyvos J., On the Temperature Dependence of Photovoltaic Module Electrical Performance: A Review Of Efficiency/Power Correlations, *Solar Energy*, **83(5)**: 614-624 (2009).

[28] Qiu Z., Zhao X., Li P., Zhang X., Ali S., Tan J., Theoretical Investigation of the Energy Performance of a Novel MPCM (Microencapsulated Phase Change Material) Slurry Based PV/T Module, *Energy*, (2015).

[29] Bergman T.L., Incropera F.P., DeWitt D.P., Lavine A.S., "Fundamentals of Heat and Mass Transfer", John Wiley & Sons Inc., 2011.

[30] Kolahan A., Maadi S.R., Teymouri Z., Schenone C., Blockchain-Based Solution for Energy Demand-Side Management of Residential Buildings, *Sustainable Cities and Society*, **75**: 103316 (2021).

[31] Yazdanifard F., Ebrahimnia-Bajestan E., Ameri M., Performance of a Parabolic trough Concentrating Photovoltaic/Thermal System: Effects of Flow Regime, Design Parameters, and Using Nanofluids, *Energy Conversion and Management*, **148**: 1265-1277 (2017).

[32] Daungthongsuk W., Wongwises S., A Critical Review of Convective Heat Transfer of Nanofluids, *Renewable and Sustainable Energy Reviews*, **11(5)**: 797-817 (2007).

[33] Maadi S.R., Khatibi M., Ebrahimnia-Bajestan E., Wood D., A Parametric Study of a Novel PV/T System Model Which Includes the Greenhouse Effect, "*IEA SHC International Conference on Solar Heating and Cooling for Buildings and Industry*", Santiago, Chile (2019).

[34] Saray J.A., Heyhat M.M., Modeling of a Direct Absorption Parabolic trough Collector Based on using Nanofluid: 4E Assessment and Water-Energy Nexus Analysis, *Energy*, 123170 (2022).

[35] Yazdanpanahi J., Sarhaddi F., Adeli M.M., Experimental Investigation of Exergy Efficiency of a Solar Photovoltaic Thermal (PVT) Water Collector Based on Exergy Losses, *Solar Energy*, **118**: 197-208 (2015).

[36] Kolahan A., Maadi S., Passandideh M. Fard, Sardarabadi M., "Numerical and Experimental Investigations on the Effect of Adding Nanoparticles on Entropy Generation in PVT Systems", *17th Conference On Fluid Dynamics, fd2017* (2017).

[37] Sardarabadi M., Passandideh-Fard M., Zeinali Heris S., Experimental Investigation of the Effects of Silica/Water Nanofluid on PV/T (Photovoltaic Thermal Units), *Energy*, **66**: 264-272 (2014).